catalysts

MDPI

Article

Insight into Structural and Physicochemical Properties of ZrO_2-SiO_2 Monolithic Catalysts with Hierarchical Pore Structure: Effect of Zirconium Precursor

Katarzyna Maresz [1], Agnieszka Ciemięga [1,*], Patryk Bezkosty [2], Kamil Kornaus [2], Maciej Sitarz [2], Maciej Krzywiecki [3] and Julita Mrowiec-Białoń [1,*]

[1] Institute of Chemical Engineering Polish Academy of Sciences, Bałtycka 5, 44-100 Gliwice, Poland; maresz@iich.gliwice.pl
[2] Faculty of Materials Science and Ceramics, AGH University of Science and Technology, A. Mickiewicza 30 Avenue, 30-059 Cracow, Poland; bezkosty@agh.edu.pl (P.B.); kornaus@agh.edu.pl (K.K.); msitarz@agh.edu.pl (M.S.)
[3] Institute of Physics, CSE, Silesian University of Technology, Konarskiego 22B, 44-100 Gliwice, Poland; maciej.krzywiecki@polsl.pl
* Correspondence: ciemiega@iich.gliwice.pl (A.C.); j.bialon@iich.gliwice.pl (J.M.-B.)

Abstract: Zirconia–silica monolithic catalysts with hierarchical micro/macroporous structure were obtained in a sol-gel process combined with phase separation using inorganic salts, i.e., oxychloride, oxynitrate and sulphate, as a zirconium source. It was found that the use of zirconium oxychloride and prehydrolysis of tetraethoxysilane (TEOS) resulted in materials characterized by a well-developed continuous structure of macropores with a diameter of ca. 10 µm. For zirconium oxynitrate and sulfate modified materials, the prehydrolysis hardly affected the macropore size. The micropores with a diameter of 1.5 nm in the skeleton of all materials provided a large surface area of 550–590 m^2/g. A high dispersion of zirconia in the silica skeleton in all studied materials was shown. However, the largest surface concentration of Lewis and Brönsted acid sites was found in the monolith synthesized with zirconium oxychloride. The monoliths were used as a core for continuous-flow microreactors and high catalytic activity was confirmed in the deacetalization of benzylaldehyde dimethyl acetal. The process was characterized by a high efficiency at low temperature, i.e., 35 °C.

Keywords: zirconia–silica hierarchical monoliths; porosity; diffusion; catalytic activity

Citation: Maresz, K.; Ciemięga, A.; Bezkosty, P.; Kornaus, K.; Sitarz, M.; Krzywiecki, M.; Mrowiec-Białoń, J. Insight into Structural and Physicochemical Properties of ZrO_2-SiO_2 Monolithic Catalysts with Hierarchical Pore Structure: Effect of Zirconium Precursor. *Catalysts* **2023**, *13*, 1516. https://doi.org/10.3390/catal13121516

Academic Editor: Nicolas Abatzoglou

Received: 29 November 2023
Revised: 13 December 2023
Accepted: 14 December 2023
Published: 16 December 2023

1. Introduction

Inorganic monolithic materials with hierarchical pore structure have received considerable attention due to their interesting structural and flow characteristics. The skeleton of these materials is similar to the open-cell foams used in heat exchangers, absorbers and structured catalysts, but the dimensions are reduced to the microscale (Figure S1). These materials are characterized by a large specific surface area that can be functionalized with various active species, and they open a wide range of practical uses in catalysis, sorption and separation processes. Their characteristic feature is a well-developed network of micro- and mesopores connected to flow-through macropores. Silica materials with such properties can be fabricated using the method proposed by Nakanishi et al. [1] and developed by other scientists [2–4]. On the whole, the synthesis procedure combines phase separation of the water-soluble polymer and the formation of the silica skeleton in the sol-gel process. A polymer, mostly poly(ethylene oxide) or polyethylene glycol, acts both as a porogen of larger pores and as a phase-separation inducer. The key issue for controlling the morphology of the resulting material is to fit phase separation and gelation kinetics. Moreover, the structural properties strongly depend on the ageing process and post-synthesis hydrothermal treatment in aqueous ammonia solution [5]. This method was originally designed for the synthesis of silica monolithic capillaries for high-performance liquid chromatography

columns [6], and next, it was used in the fabrication of microreactor cores [7]. Modification of the synthesis method allows one to obtain materials with specific textural characteristics, which is extremely important in catalyst design. Incorporation of catalytic species can be carried out using a post-synthesis surface modification or in the one-step procedure, i.e., co-condensation of silica and metal oxide precursors. The post-synthesis method has already been successfully applied in the preparation of continuous-flow monolithic microreactors with different active species, including enzymes [8,9], titania [10], zirconia [11], alumina [7,12], sulfonic acid groups [5] and amino groups [7,13]. Application of this method allows one to preserve the pristine macroporous structure of the silica support, which is not observed in the one-step method. The introduction of an additional component into the reaction mixture was shown to have a strong effect on the rate of the sol-gel process and phase separation, and thus, on the final structure of monoliths, which has been demonstrated for zirconia–silica [14,15] and titania–silica mixed oxides [10]. In both types of monoliths, a significant decrease in the size of mesopores and macropores was observed, and lower porosity translated directly into higher flow resistance. However, titania–silica materials were characterized by better dispersion of the active species in the skeleton and better stability of catalytic properties than those modified with the impregnation method. This was confirmed by a high efficiency in the selective oxidation of 1,3,5-trimethylphenol with H_2O_2 [10].

Here, we focused on zirconia–silica monoliths with hierarchical pore structure for continuous-flow catalytic processes, and their synthesis has been directed towards obtaining materials with improved porosity using the co-condensation method, which is still a challenge. The aim of this work was to study the impact of a type of zirconium salt on the structure and physicochemical properties of zirconia–silica monoliths. Materials with a bimodal pore size distribution and large surface area were synthesized using three inorganic zirconium salts, i.e., oxychloride, oxynitrate and sulphate, as a zirconium source and a modified sol-gel process combined with phase separation. The dispersion of zirconium atoms in the silica skeleton and surface acidity were studied with spectroscopic methods. Furthermore, the flow properties of the monoliths were investigated. Finally, the materials were used as a core of microreactors and tested for their suitability in the deacetalization of benzaldehyde dimethyl acetal. This reaction often represents the initial step of a tandem process involving the deacetalization and Knoevenagel condensation reactions [16].

2. Results and Discussion

The objective of this study was to investigate the effect of the type of inorganic zirconium salt on the properties of monolithic zirconia–silica materials with hierarchical pore structure. Three zirconium salts, i.e., sulfate, oxynitrate and oxychloride, were applied in a one-step synthesis of binary oxide with a fixed mass ratio of Zr/SiO_2 equal to 0.02. A detailed analysis of SEM images of cylindrical materials (4 × 40 mm) showed that in the case of zirconium oxychloride, the diameters of the macropores varied in size and decreased along the length of the monolith from top to bottom (Figure 1). A change in skeleton structure was also observed, i.e., the thickness of the walls and struts in the lower part was clearly thinner and was similar to the structure of silica titanium monoliths [10].

In contrast, the upper part resembled those found in pure silica monoliths. This suggested a non-uniform distribution of zirconium precursor in the whole volume of the sample. Such heterogeneity of the gel structure has not been encountered in our previous studies, either for pure silica monoliths or for titania–silica materials. Therefore, an attempt was made to obtain monoliths of homogeneous porosity. The goal was achieved with the application of the prehydrolysis of TEOS, which was carried out at room temperature for 4 h prior to the addition of the zirconium oxychloride. This approach was tested for two other salts. The results of these studies are shown below.

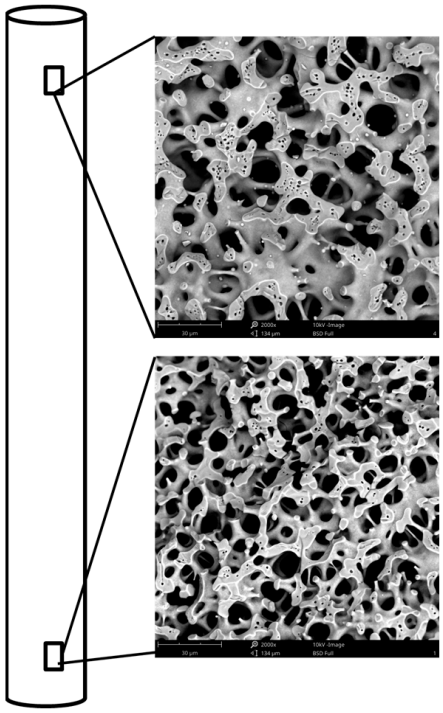

Figure 1. SEM images of Zr/Si-Cl sample—top and bottom part of the monolith.

A detailed analysis of the SEM images (Figure 2) and mercury porosimetry data (Figure 3) showed a complex relationship between the structural properties of the materials and the type of salt and synthesis method. The size of the macropores depended significantly on the type of zirconium salt and an increase in the pore diameter was observed in the following order: oxynitrate < sulphate < oxychloride (Figure 3, Table 1). A similar relation was seen for the total pore volume (V_t). Furthermore, differences in the skeletal structure of the monoliths are visible in the SEM images.

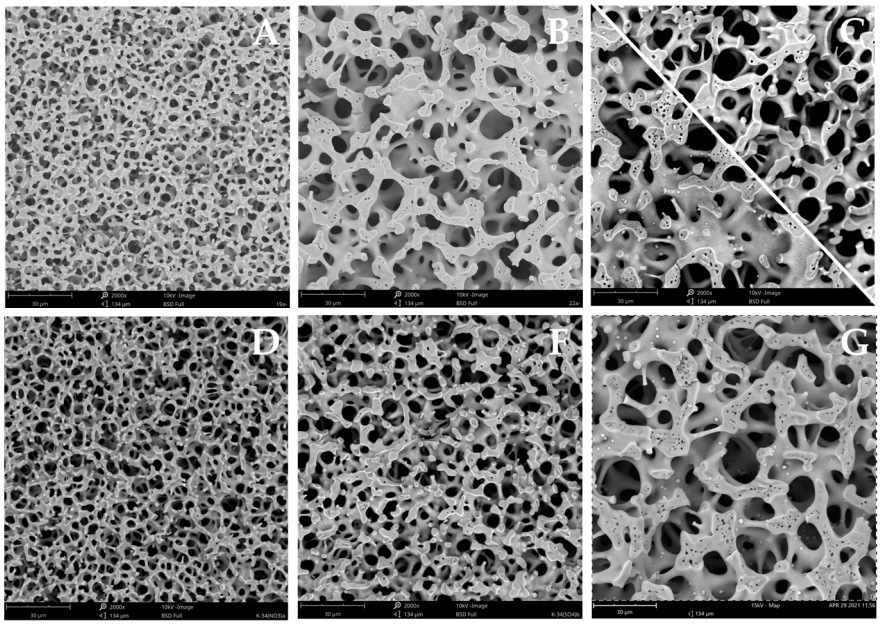

Figure 2. SEM images of samples synthesized without prehydrolysis: Zr/Si-N (**A**); Zr/Si-S (**B**); Zr/Si-Cl (**C**), and with prehydrolysis: Zr/Si-N-h (**D**); Zr/Si-S-h (**E**); Zr/Si-Cl-h (**F**).

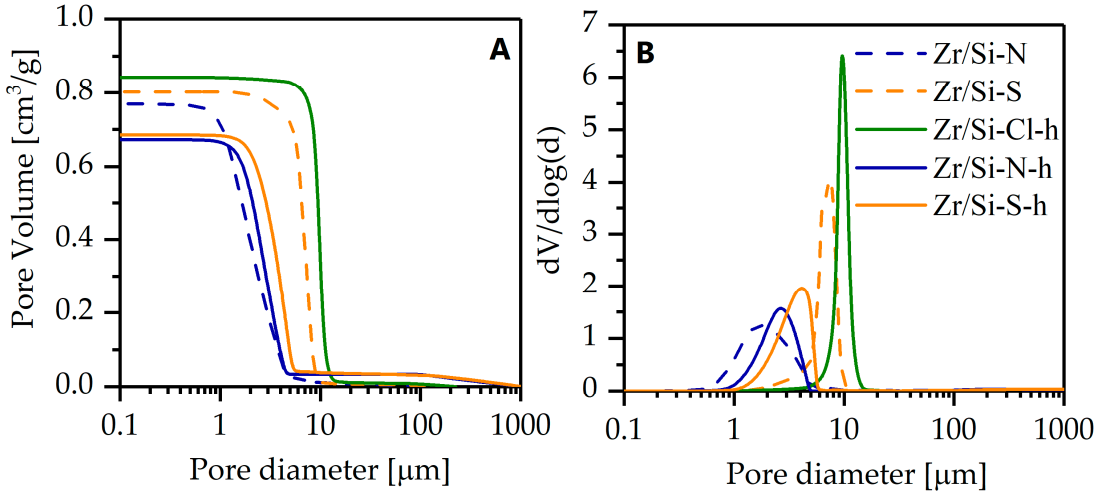

Figure 3. Cumulative pore volume (**A**) and macropore size distribution (**B**) of zirconia–silica monoliths.

Table 1. Structure parameters of zirconia–silica monoliths.

Sample	S_{BET} [m^2/g]	V_{micro} [cm^3/g]	S_D [m^2/g]	V_t [cm^3/g]	d_{micro} [nm]	ρ_s [g/cm^3]	d_{macro} [μm]
Zr/Si-Cl-h	547	0.26	623	0.84	1.5	2.042	10.2
Zr/Si-N	592	0.29	664	0.77	1.5	2.049	1.8
Zr/Si-N-h	574	0.28	649	0.67	1.5	2.050	2.5
Zr/Si-S	559	0.27	633	0.81	1.5	2.051	7.5
Zr/Si-S-h	564	0.27	637	0.68	1.5	2.048	5.0

V_{micro}—micropore volume; S_D—surface area calculated from Dubinin–Astakhov equation; V_t—total pore volume; d_{micro} and d_{macro}—micropore and macropore diameter, respectively (maximum of the pore size distribution); ρs—skeletal density.

In the sample Zr/Si-S the thickness of the skeleton walls (struts) was significantly greater than in Zr/Si-N (Figure 2A,B). The influence of the TEOS prehydrolysis in the case of samples synthesized using zirconium oxynitrates (Zr/Si-N and Zr/Si-N-h) was negligible; a small shift of the pore size distribution curve to larger pores and a ca. 15% decrease in total pore volume were recorded in the Zr/Si-N-h sample (Figure 3B, Table 1). The structure of the skeleton for both samples was almost the same. A reverse relation was seen for the sulfate salt. In the prehydrolyzed sample, a decrease in pore diameter and pore volume was recorded, and the structure of the skeleton also changed and significantly thinner walls were detected, which were similar to those observed in the Zr/Si-N sample. The Zr/Si-Cl-h material was characterized by a very narrow macropore size distribution with a diameter of 10.2 μm and the largest total pore volume (0.84 cm^3/g). The thick walls (struts) that formed the skeleton of this sample resembled those seen in the Zr/Si-S material.

Figure S2 shows nitrogen adsorption isotherms and the pore size distribution of zirconia–silica monoliths. These materials exhibited virtually the same porosity at the nanometric scale despite the use of different zirconium precursors and synthesis methods. The nitrogen adsorption isotherms of type I, according to the IUPAC classification, indicated a microporous structure of the skeletal struts that contain pores with a diameter of ca. 1.5 nm. All samples exhibited a high specific surface area (550–600 m^2/g) and small (ca. 0.3 cm^3/g) micropore volume. The skeletal density of all samples, ca. 2.05 g/cm^3, is typical for silica-based materials obtained using the sol-gel method.

The nature of the interaction between the zirconium ions and silica skeleton in the binary oxides was studied with various techniques. XRD did not show the presence of a crystalline zirconia phase in all samples. A representative spectrum of the Zr/Si-Cl-h material is shown in Figure S3. Only a broad band in the range of 15–40 2θ was

recorded, which is characteristic of amorphous silica. The analysis of the images obtained using EDS indicated a very uniform dispersion of zirconium atoms in the silica matrix (Figure S4). Furthermore, the UV spectra of the samples were almost identical (Figure S5). The maximum absorption at 207 nm can be attributed to the presence of small oligomers of zirconium oxide, and no bulk-like zirconium oxide phases were present on the silica surface, in agreement with the XRD results.

The FTIR spectra were similar for three zirconia–silica samples (Figure 4). These spectra did not show the characteristic band at 3742 cm^{-1} for isolated surface hydroxyls, which was very well seen for pure silica; this may indicate the formation of Si-O-Zr bonds. The incorporation of zirconium into the silica skeleton was analyzed in the 910–960 cm^{-1} region where the Zr-O-Si vibrations appear [17].

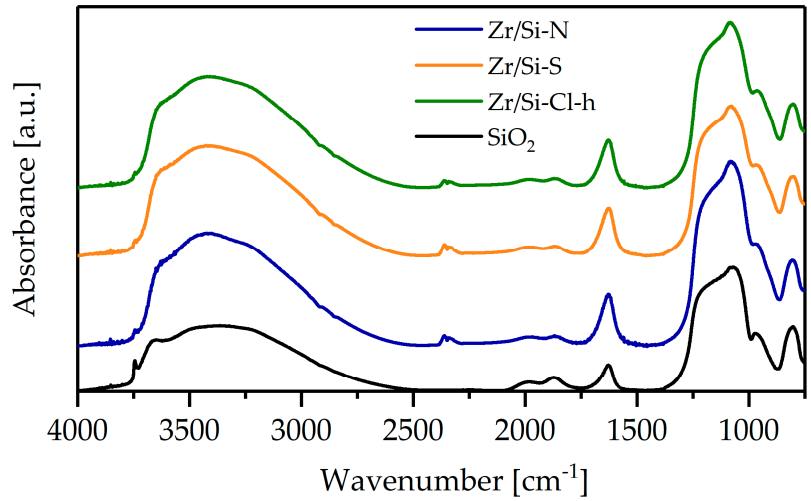

Figure 4. FTIR spectra of silica and zirconia-silica monoliths.

Deconvolution of the spectra was performed in the range of 1400–700 cm^{-1} to extract the Zr-O-Si connectivity band at 940 cm^{-1} (orange) and Si-O-Si bands at 1228 (blue) and 1186 cm^{-1} (green) [18]. A representative spectrum of Zr/Si-Cl-h sample after deconvolution is shown in Figure 5.

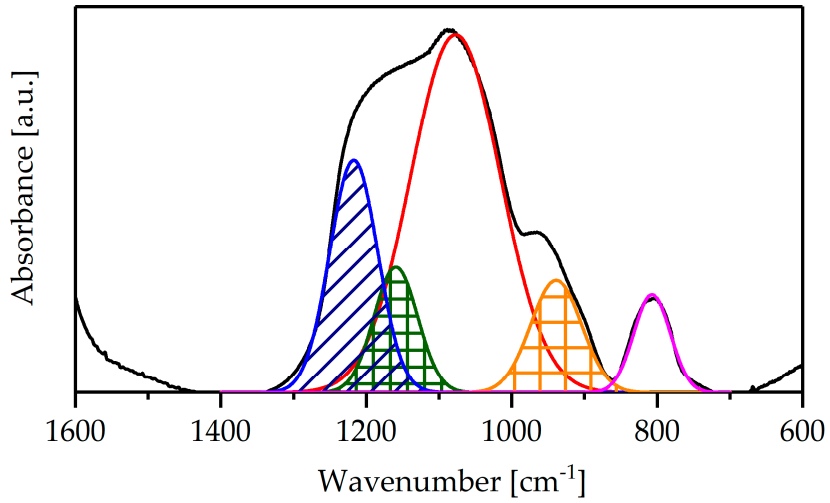

Figure 5. FTIR spectrum of Zr/Si-Cl-h monoliths: pristine (black) and after deconvolution.

The semi-quantitative value of the zirconium dispersion was obtained using expression (1) [19]:

$$D_{(Zr\text{-}O\text{-}Si)} = [S_{(Zr\text{-}O\text{-}Si)}/(S_{(Si\text{-}O\text{-}Si)}]x_{Si}/x_{Zr} \quad (1)$$

where $S_{(Zr\text{-}O\text{-}Si)}$ is the area of the fitted band at 940 cm^{-1}, $S_{(Si\text{-}O\text{-}Si)}$ is the sum of the band area at approximately 1228 and 1186 cm^{-1} and x_{Si}/x_{Zr} is the molar ratio of Si/Zr. The highest dispersion value was found in the Zr/Si-Cl-h sample (Table 2); it was ca. 10% and 27% higher than those determined for samples synthesized with the use of zirconium oxynitrate and zirconium sulfate, respectively.

Table 2. Data from FTIR studies: $D_{(Zr\text{-}O\text{-}Si)}$—zirconium dispersion in silica skeleton and relative surface area of characteristic bands of the Lewis and Brönsted acid sites.

Sample	Dispersion $D_{(Zr\text{-}O\text{-}Si)}$	Concentration [μm/g]		
		Lewis Acid Sites (L) (1446 cm^{-1})	Brönsted Acid Sites (B) (1544 cm^{-1})	B\L
Zr/Si-Cl-h	26.4	808	64	0.079
Zr/Si-N	24.1	190	20	0.105
Zr/Si-S	20.7	633	9	0.014

The acidic properties of zirconia–silica materials were determined from FTIR spectra collected after pyridine adsorption (Figure 6).

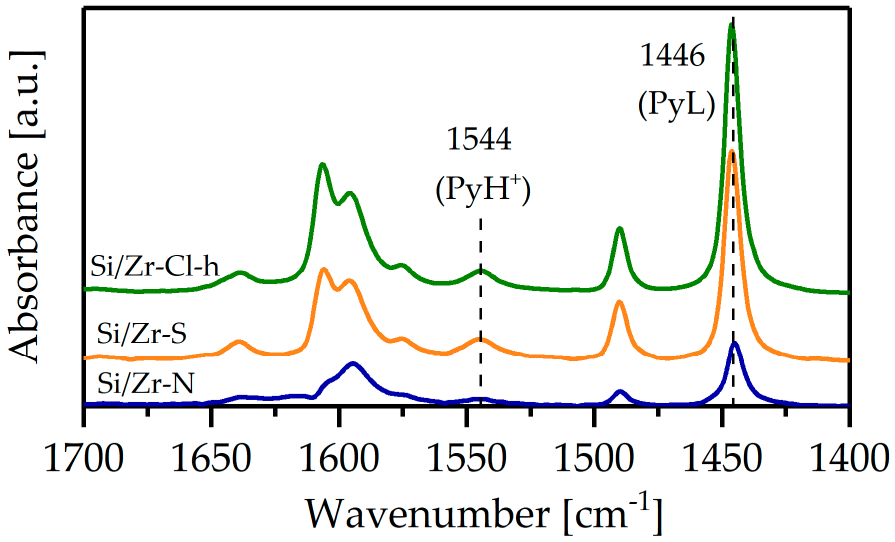

Figure 6. FTIR spectra of zirconia-silica monoliths after pyridine adsorption.

Si-Zr mixed oxides form both Brönsted and Lewis acid sites, whereas pure ZrO_2 exhibits only Lewis acidity [20]. The characteristic band of pyridine adsorbed on the Lewis (1446 cm^{-1}) and Brönsted sites (1544 cm^{-1}) were indicated in the spectra and the calculated values of site concentration are collected in Table 2. The surface concentration of the Lewis and Brönsted acid sites in the monolith Zr/Si-Cl-h was substantially higher than that found in the Zr/Si-N and Zr/Si-S samples. Moreover, the higher ratio of PyH^+ to PyL acid centers in the Zr/Si-Cl-h sample corroborates well the value of zirconium ion dispersion in the silica matrix.

Figure 7 shows the XPS core-level spectra of Zr3d, Si2p and O1s. The Zr3d spectrum was a doublet $Zr(3d_{5/2})$-$Zr(3d_{3/2})$ and the binding energy of $Zr(3d_{5/2})$ was equal to 183.34, 183.57 and 183.87 eV for Zr/Si-N, Zr/Si-S and Zr/Si-Cl-h, respectively, and was higher than that found for pure crystalline zirconia (181.94 eV) [21].

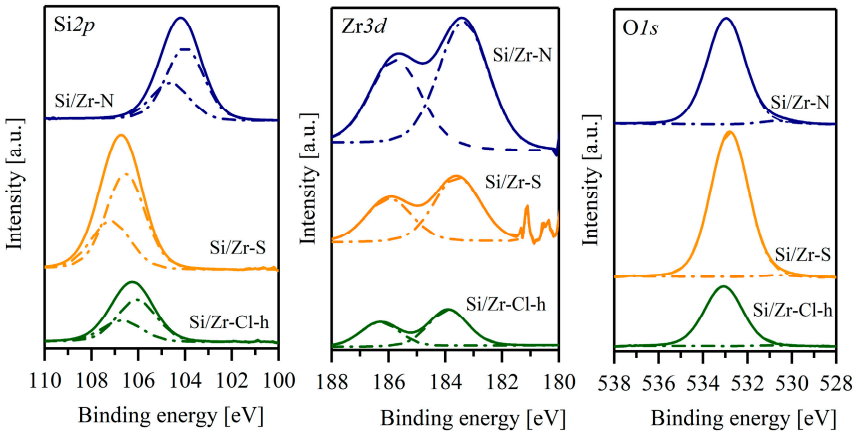

Figure 7. XPS spectra of samples.

A shift in the binding energy of the $Zr(3d_{5/2})$ band to higher values can be attributed to the smaller relaxation energy for highly dispersed zirconium oxide species [22]. Moreover, the broadening of the Zr 3d peak and the greater distance between the $Zr(3d_{5/2})$ and $Zr(3d_{3/2})$ peaks for the samples synthesized from nitrate and sulphate salts showed that these samples exhibit a less-homogeneous chemical environment around Zr^{4+} than the Zr/Si-Cl-h sample [23]. The measured binding energy of the Si2p core level of these materials was 104, 106.5 and 106 eV, which could indicate a more defective SiO_2 structure in the Zr/Si–S and Zr/Si-Cl-h samples than in Zr/Si-N. It should be mentioned that in pure silica the binding energy of Si2p is equal to 103 eV [21]. The O1s XPS spectra are presented in Figure 7. The peak at 533 eV should be assigned to the Si-O-Si unit. The spectrum of Zr/Si-N showed an extra weak peak at 530.5 eV that may be attributed to Zr-O-Zr units, which was not visible in the two other samples studied. This may indicate that the ZrO_2 nanooligomers in this material were slightly larger.

The use of monolithic materials with an open flow-through structure as the core for continuous-flow microreactors requires their flow characteristics, because they directly translate to operating costs. Therefore, the flow properties of the obtained zirconia–silica monoliths were investigated. A linear relation of pressure drop vs. flow rate was obtained (Figure 8), and the permeability coefficient was calculated using the Darcy–Weisbach Equation (2) [24]:

$$(\Delta P)/L = \eta \cdot V \cdot 10^{-9}/(K \cdot A) \quad (2)$$

where $\Delta P/L$ [bar/cm] is the pressure drop gradient, V is the volumetric flow rate of liquid [cm^3/s], η is the viscosity [Pas·s], A is the cross-sectional area of the monolith [cm^2] and K is the the permeability coefficient [m^2].

The values of the permeability coefficient correlate well with the diameter (d) of the flow-through macropores (see Table 1 and the inset in Figure 8), and the relation $K \sim d^2$ was confirmed.

The materials were used as a core for continuous-flow microreactors and their catalytic properties were tested in the deacetalization of benzaldehyde dimethyl acetal. Similar acetal conversions (ca. 80% at 35 °C) were obtained in all microreactors despite different concentrations of acid centers. This indicates that the number of acid centers required to achieve a high conversion was sufficient even in the sample with the lowest concentration of Brönsted sites. Moreover, the Zr/Si-Cl-h monolith was tested at higher temperatures (50 °C and 65 °C), and an increase in conversion of acetal up to the value of 86% was observed (Figure 9). The productivity of benzaldehyde reached a value of ca. 22 mmol/g·h (35 °C), which was significantly higher than those obtained in a pack-bed flow reactor equipped with sulfonic acid centers (45% conversion, 0.12 mmol/g·h conversion, temp. 60 °C) [16] and comparable to data from the batch process [25].

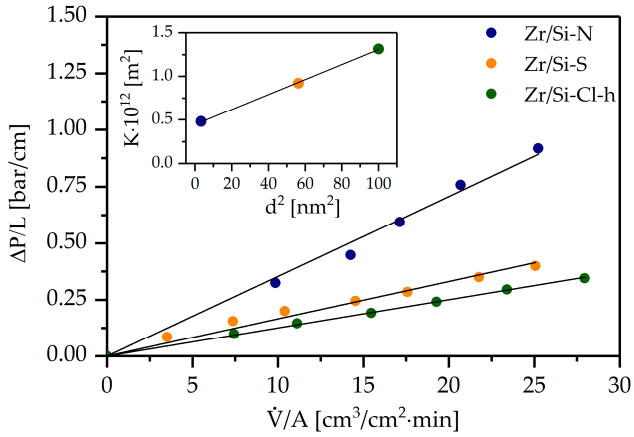

Figure 8. Pressure drop vs. flow rate for zirconia–silica monoliths and permeability coefficient (K) vs. macropore diameter (d^2) (inset).

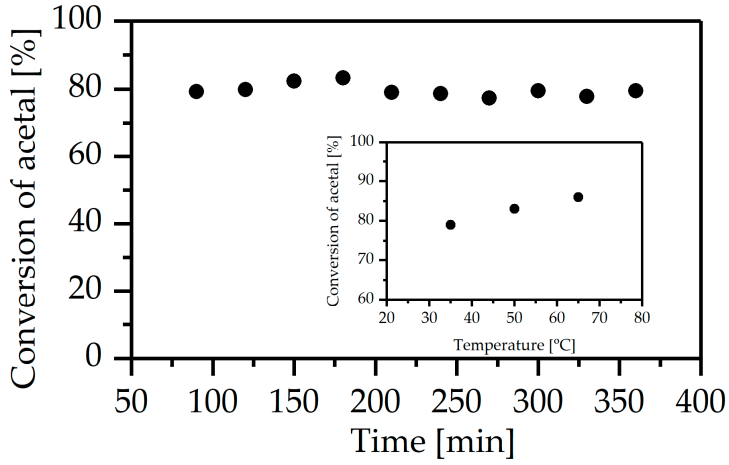

Figure 9. Conversion of benzaldehyde dimethyl acetal vs. time in Zr-Si/Cl-h microreactor; average conversion of acetal vs. reaction temperature (inset).

The results presented above evidently showed the strong influence of the type of zirconium precursor on the physicochemical and structural properties of the monoliths. In the case of zirconium oxychloride, not only was an impact on the structure observed but also a disruption of the gelation process was noticed, and it resulted in a heterogeneous macropore structure along the length of the cylindrical monoliths. However, the prehydrolysis of TEOS prior to the addition of the Zr precursor allowed us to avoid structural inhomogeneity. Moreover, it was shown that prehydrolysis hardly influenced the structure of monoliths synthesized with the use of oxynitrate and sulfate. Regarding the application in catalytic processes, the concentration of acid centers is of particular importance. The Zr/Si-Cl-h material was found to have a significantly higher concentration of Lewis and Brönsted acidic centers than those synthesized with the other two precursors. It seems that this behavior can be explained by comparing the species of zirconium salts in aqueous solutions. All three salts exist in aqueous solutions as oligomeric species. However, zirconium oxychloride forms a cyclic cation with the formula $[Zr_4(OH)_8(H_2O)_{16}]^{8+}$ in which four Zr^{4+} ions are linked by pairs of OH- ions to form a ring, while oxynitrate and sulfate are present as polymeric zig-zag chains, which are held together by sulfate and nitrate ions [26,27]. The synthesis of monoliths was carried out under acidic conditions, and the silica species formed during hydrolysis and condensation were positively charged [28], so the interaction between them and the cyclic zirconium cations during the silica skeleton building process was limited. Therefore, more zirconium species were present in the aqueous phase and probably most of them were deposited on the silica surface during the

drying process, which is consistent with the concentration of acid centers determined with pyridine adsorption measurements.

3. Materials and Methods

3.1. Reagents

Tetraethoxysilane (TEOS, 99% wt.%, ABRC, Germany), polyethylene glycol (PEG 35000, Sigma Aldrich, USA), nitric acid (65 wt.% Avantor, Poland), cetyltrimethylammonium bromide (CTAB, Sigma Aldrich), $ZrOCl_2 \cdot 8H_2O$ (Alfa Aesar, USA), $ZrO(NO_3)_2 \cdot 6H_2O$ (Sigma Aldrich) and $Zr(SO_4)_2 \cdot 4H_2O$ (Alfa Aesar) were used in the synthesis of zirconia–silica mixed oxides.

3.2. Synthesis of Monoliths

Zirconia–silica monoliths were obtained in a one-step process using the combined sol-gel method and phase separation [10]. Mixed oxides were synthesized using two approaches. In the first, 1.04 g of polyethylene glycol was dissolved in 12 cm^3 of 1 M nitric acid at room temperature. The mixture was then cooled in an ice bath and TEOS (10 cm^3) was added dropwise. The sol was stirred until a transparent, homogeneous solution was obtained. Then, 0.46 g of CTAB was poured into the flask, followed by the addition of zirconium salt. The clear mixture was loaded into polypropylene molds, sealed, allowed to gel and aged at 40 °C for 8 days (Figure 2A). The monolithic materials were washed in an excess of deionized water, dried at 40 °C and calcined at 550 °C for 8 h. In the second method, salt addition was preceded by prehydrolysis of tetraethoxysilane. Here, TEOS was added to the polyethylene glycol solution in 1M nitric acid and stirred at room temperature for 4 h. Then, CTAB and zirconium salt were added. The subsequent steps were the same as described above. Three zirconium salts were used in the synthesis of mixed oxides: $ZrOCl_2 \cdot 8H_2O$, $ZrO(NO_3)_2 \cdot 6H_2O$ and $Zr(SO_4)_2 \cdot 4H_2O$. The sample description is given in Table 3. In all materials, the mass ratio of Zr/SiO_2 was equal to 0.02.

Table 3. Sample description.

Sample	Zr Precursor	Prehydrolysis of TEOS
Zr/Si-Cl	$ZrOCl_2 \cdot 8H_2O$	no
Zr/Si-Cl-h	$ZrOCl_2 \cdot 8H_2O$	yes
Zr/Si-N	$ZrO(NO_3)_2 \cdot 6H_2O$	no
Zr/Si-N-h	$ZrO(NO_3)_2 \cdot 6H_2O$	yes
Zr/Si-S	$Zr(SO_4)_2 \cdot 4H_2O$	no
Zr/Si-S-h	$Zr(SO_4)_2 \cdot 4H_2O$	yes

3.3. Characterization

The structural parameters of the monoliths—pore size distribution, micropore volume and specific surface area—were determined from nitrogen adsorption isotherms obtained at −196 °C. Prior to analysis, the samples were degassed at 200 °C under vacuum for 24 h. The specific surface area of the materials was calculated using the standard equation proposed by Braunauer, Emmet and Teller (BET), while the micropore size was obtained from the Dubinin–Astakhov equation. The total pore volume and macropore distribution were obtained from mercury porosimetry (Quantachrome Poremaster 33 instrument). The measurements were carried out in a pressure range of 0.2–33,000 psi. To explore the macropore structure and the chemical composition of the prepared samples, Phenom XL (Thermo Fisher Scientific, Waltham, MA, USA) equipped with an electron dispersive spectroscopy (EDS) system was used. Before imaging, all samples were coated with a thin gold layer (3 nm) using an EM ACE200 vacuum coater (Leica, Wetzlar, Germany) for better conductivity. A back-scattered electron detector and an acceleration voltage of 10 kV were applied for SEM images. The EDS mapping was performed with the same detector and increased the acceleration voltage to 15 kV. A helium pycnometer (Micromeritics, USA) was used for skeletal density measurements.

FTIR spectra of mixed oxides were recorded with a NICOLET 6700 spectrometer (Thermo Fisher Scientific) using the KBr technique (pellet: 5% of sample in KBr). Measurements were carried out in the range of 650–4000 cm^{-1} with a resolution of 4 cm^{-1}.

The acidic properties of the samples were determined using an FTIR spectrometer (Invenio, Bruker, MCT detector) and pyridine as the probe molecule. The samples were pressed into pellets at p = 3 bar. Activation of the samples was carried out at 200 °C. Next, the samples were cooled to 150 °C and contacted with pyridine vapor. After 10 min, physisorbed molecules were desorbed at the same temperature. Spectra were recorded at 150 °C in the range of 4000–600 cm^{-1} and 100 scans were taken for each sample at a resolution of 2 cm^{-1}. The acid center concentrations were calculated from the intensity of the pyridine bands associated with the Brønsted (1544 cm^{-1}, PyH^+) and Lewis (1446 cm^{-1}, PyL) sites, and values of the absorption coefficients of 0.07 cm/μmol and 0.10 cm/μmol were used, respectively [29].

XRD measurements were performed on a Philips/Panalytical X'Pert ProMD powder diffractometer (Malvern Panalytical, Malvern, UK) in standard Bragg–Brentano geometry using CuKα radiation.

XPS investigations were carried out with a PREVAC EA15 hemispherical electron energy analyzer equipped with a 2D-MCP detector (system base pressure 8×10^{-9} Pa). The samples were excited with an energy of 1486.60 eV provided by Al-Kα radiation (PREVAC dual-anode XR-40B source). The pass energy was set to 200 eV (with scanning step 0.9 eV) for the survey spectra and to 100 eV (with scanning step 0.05 eV) for particular energy regions. Measurements were made with a normal take-off angle. The binding energy scale of the analyzer was calibrated to Au $4f_{7/2}$ (84.0 eV) [30]. The data obtained were quantified using CASA XPS® embedded algorithms and relative sensitivity factors [31]. The Shirley function was used for background subtraction. The particular components were fitted with a sum of Gaussian (70%) and Lorentzian (30%) lines. The full width at half maximum (FWHM) values for the peaks at the similar binding energy region were allowed to vary within a narrow range for residual line minimization. The uncertainty of determining the position of the energy was estimated at 0.11 eV.

The catalytic properties of acid centers were verified in the deacetalization reaction of benzylaldehyde dimethyl acetal, which was carried out in a continuous-flow microreactor under the following conditions: temperature—35 °C, 50 °C, 65 °C; flow rate—0.03 cm^3/min; solvent acetonitrile, acetal concentration—2.4 mmol/cm^3; molar ratio acetal:H_2O—1:1.

4. Conclusions

Three inorganic zirconium salts, i.e., oxychloride, oxynitrate and sulfate, were used in the synthesis of zirconia–silica monoliths with a hierarchical pore structure and a Zr/SiO_2 mass ratio of 0.02. An inspection of the structural and physicochemical properties of the synthesized materials clearly indicated that the use of oxychloride and prehydrolysis of TEOS allowed us to obtain materials with the largest volume and diameter of macropores and the thickest skeleton walls. Moreover, these monoliths featured significantly higher surface concentrations of Brönsted and Lewis acidic centers. It was shown that prehydrolysis hardly influenced the macroporous structure of monoliths synthesized with the use of oxynitrate and sulfate. Regardless of the zirconium precursor applied in the synthesis, micropores with a diameter of 1.5 nm were present in the skeleton of all materials, and their specific surface area was in the range of 550–590 m^2/g. A high dispersion of zirconium in the silica skeleton was confirmed in all monoliths. The catalytic properties of acid centers in the monoliths were verified in the deacetalization reaction of benzaldehyde dimethyl acetal performed in continuous-flow microreactors. All materials exhibited similarly high catalytic activity despite the concentration of acid centers. However, the best flow properties arising from the largest size of macropores were obtained for the monolith synthesized using zirconium oxychloride. The results open the possibility of their further functionalization, for example, with the attachment of amino groups and use in the deacetalization-Knoevenagel tandem reaction.

Supplementary Materials: The following supporting information can be downloaded at: https://www.mdpi.com/article/10.3390/catal13121516/s1, Figure S1: SEM images of ceramic foam and silica micro-foam; Figure S2: Cumulative pore volume and macropore size distribution of zirconia-silica monoliths; Figure S3: XRD spectrum of Zr/Si-Cl-h sample; Figure S4: SEM-EDS mapping images of Zr/Si-Cl-h; Zr/Si-N and Zr/Si-S; Figure S5: UV-Vis spectra of SiO_2-ZrO_2 monoliths.

Author Contributions: Conceptualization, K.M., A.C. and J.M.-B.; investigation, K.M., A.C., P.B., K.K., M.S. and M.K.; writing—original draft preparation, K.M. and A.C.; writing—review and editing, J.M.-B.; visualization, A.C.; supervision, J.M.-B.; project administration, A.C. All authors have read and agreed to the published version of the manuscript.

Funding: This research was funded by the National Science Centre, Poland, grant number 2021/43/D/ST8/01727.

Data Availability Statement: Data will be made available on request.

Acknowledgments: The authors acknowledge the Electron Spectroscopies and Functional Materials (ESpeFuM) laboratory (at the Institute of Physics—CSE, Silesian University of Technology) for access to the XPS experimental setup.

Conflicts of Interest: The authors declare no conflict of interest.

References

1. Nakanishi, K.; Takahashi, R.; Nagakane, T.; Kitayama, K.; Koheiya, N.; Shikata, H.; Soga, N. Formation of hierarchical pore structure in silica gel. *J. Sol-Gel Sci. Technol.* **2000**, *17*, 191–210. [CrossRef]
2. Smatt, J.H.; Schunk, S.; Linden, M. Versatile double-templating synthesis route to silica monoliths exhibiting a multimodal hierarchical porosity. *Chem. Mater.* **2003**, *15*, 2354–2361. [CrossRef]
3. Pudło, W.; Gawlik, W.; Mrowiec-Białoń, J.; Buczek, T.; Malinowski, J.J.; Jarzębski, A.B. Materials with multimodal hierarchical porosity. *Inz. Chem. Proces.* **2006**, *27*, 177–185.
4. El-Naggar, I.M.; Mowafy, E.A.; El-Aryan, Y.F.; Abd El-Wahed, M.G. Sorption mechanism for Cs^+, Co^{2+} and Eu^{3+} on amorphous zirconium silicate as cation exchanger. *Solid State Ion.* **2007**, *178*, 741–747. [CrossRef]
5. Ciemięga, A.; Maresz, K.; Malinowski, J.J.; Mrowiec-Białoń, J. Continuous-flow monolithic silica microreactors with arenesulphonic acid groups: Structure-catalytic activity relationships. *Catalysts* **2017**, *7*, 255. [CrossRef]
6. Tanaka, N.; Kobayashi, H.; Nakanishi, K.; Minakuchi, H.; Ishizuka, N. Monolithic LC columns. *Anal. Chem.* **2001**, *73*, 420A–429A. [CrossRef]
7. El Kadib, A.; Chimenton, R.; Sachse, A.; Fajula, F.; Galarneau, A.; Coq, B. Functionalized inorganic monolithic microreactors for high productivity in fine chemicals catalytic synthesis. *Angew. Chem. Int. Ed.* **2009**, *48*, 4969–4972. [CrossRef]
8. Hou, C.M.; Gheczy, N.; Messmer, D.; Szymańska, K.; Adamcik, J.; Mezzenga, R.; Jarzębski, A.B.; Walde, P. Stable immobilization of enzymes in a macro- and mesoporous silica monolith. *ACS Omega* **2019**, *4*, 7795–7806. [CrossRef]
9. Kowalczykiewicz, D.; Przypis, M.; Mestron, L.; Tischler, D.; Hagedoorn, P.-L.; Hanefeld, U.; Jarzębski, A.; Szymańska, K. Engineering of continuous bienzymatic cascade process using monolithic microreactors—In flow synthesis of trehalose. *Chem. Eng. J.* **2021**, *427*, 131439. [CrossRef]
10. Koreniuk, A.; Maresz, K.; Odrozek, K.; Mrowiec-Białoń, J. Titania-silica monolithic multichannel microreactors. Proof of concept and fabrication/structure/catalytic properties in the oxidation of 2,3,6-trimethylphenol. *Microporous Mesoporous Mater.* **2016**, *229*, 98–105. [CrossRef]
11. Ciemięga, A.; Maresz, K.; Mrowiec-Białoń, J. Monolithic microreactors of different structure as an effective tool for in flow MPV reaction. *Chem. Eng. J.* **2020**, *379*, 122281.
12. Ciemięga, A.; Maresz, K.; Mrowiec-Białoń, J. Meervein-Ponndorf-Vereley reduction of carbonyl compounds in monolithic siliceous microreactors doped with Lewis acid centres. *Appl. Catal. A Gen.* **2018**, *560*, 111–118. [CrossRef]
13. Turke, K.; Meinusch, R.; Cop, P.; da Costa, E.P.; Brand, R.D.; Henss, A.; Schreiner, P.R.; Smarsly, B.M. Amine-functionalized nanoporous silica monoliths for heterogeneous catalysis of the knoevenagel condensation in flow. *ACS Omega* **2021**, *6*, 425–437. [CrossRef] [PubMed]
14. Takahashi, R.; Nakanishi, K.; Soga, N. Phase separation process of polymer-incorporated silica-zirconia sol-gel system. *J. Sol-Gel Sci. Technol.* **1997**, *8*, 71–76. [CrossRef]
15. Takahashi, R.; Nakanishi, K.; Soga, N. Morphology control of macroporous silica-zirconia gel based on phase separation. *J. Ceram. Soc. Jpn.* **1998**, *106*, 772–777. [CrossRef]
16. Borah, P.; Fianchini, M.; Pericàs, M.A. Assessing the role of site isolation and compartmentalization in packed-bed flow reactors for processes involving wolf-and-lamb scenarios. *ACS Catal.* **2021**, *11*, 6234–6242. [CrossRef]
17. Miller, J.B.; Rankin, S.E.; Ko, E.I. Strategies in controlling the homogeneity of zirconia silica aerogels—Effect of preparation on textural and catalytic properties. *J. Catal.* **1994**, *148*, 673–682. [CrossRef]

18. Wu, Z.G.; Zhao, Y.X.; Liu, D.S. The synthesis and characterization of mesoporous silica-zirconia aerogels. *Microporous Mesoporous Mater.* **2004**, *68*, 127–132. [CrossRef]
19. Dutoit, D.C.M.; Schneider, M.; Baiker, A. Titania-silica mixed oxides. 1. Influence of sol-gel and drying conditions on structural-properties. *J. Catal.* **1995**, *153*, 165–176. [CrossRef]
20. Pyen, S.; Hong, E.; Shin, M.; Suh, Y.W.; Shin, C.H. Acidity of co-precipitated SiO_2-ZrO_2 mixed oxides in the acid-catalyzed dehydrations of iso-propanol and formic acid. *Mol. Catal.* **2018**, *448*, 71–77. [CrossRef]
21. Rayner, G.B.; Kang, D.; Zhang, Y.; Lucovsky, G. Nonlinear composition dependence of X-ray Photoelectron Spectroscopy and Auger Electron Spectroscopy features in plasma-deposited zirconium silicate alloy thin films. *J. Vac. Sci. Technol. B* **2002**, *20*, 1748–1758. [CrossRef]
22. Moon, S.C.; Fujino, M.; Yamashita, H.; Anpo, M. Characterization of zirconium-silicon binary oxide catalysts prepared by the sol-gel method and their photocatalytic activity for the isomerization of 2-butene. *J. Phys. Chem. B* **1997**, *101*, 369–373. [CrossRef]
23. Zhang, B.; Tang, M.H.; Yuan, J.; Wu, L. Support effect in Meerwein-Ponndorf-Verley reduction of benzaldehyde over supported zirconia catalysts. *Chin. J. Catal.* **2012**, *33*, 914–922. [CrossRef]
24. Whitaker, S. Advances in theory of fluid motion in porous media. *Ind. Eng. Chem.* **1969**, *61*, 14. [CrossRef]
25. Chen, S.; Zhang, F.W.; Yang, M.Q.; Li, X.C.; Liang, H.L.; Qiao, Y.; Liu, D.Y.; Fan, W.B. A simple strategy towards the preparation of a highly active bifunctionalized catalyst for the deacetalization reaction. *Appl. Catal. A Gen.* **2016**, *513*, 47–52. [CrossRef]
26. Wiberg, E.; Wiberg, N. *Inorganic Chemistry*; Academic Press: Cambridge, MA, USA; De Gruyter: San Diego, CA, USA; Berlin, Germany; New York, NY, USA, 2001.
27. Wong, M.S.; Huang, H.C.; Ying, J.Y. Supramolecular-templated synthesis of nanoporous zirconia-silica catalysts. *Chem. Mater.* **2002**, *14*, 1961–1973. [CrossRef]
28. Brinker, C. *Sol-Gel Science: The Physics and Chemistry of Sol-Gel Processing*; Elsevier LTD: Oxford, UK, 1990.
29. Góra-Marek, K.; Derewiński, M.; Sarv, P.; Datka, J. IR and NMR studies of mesoporous alumina and related aluminosilicates. *Catal. Today* **2005**, *101*, 131–138. [CrossRef]
30. Lindau, I.; Pianetta, P.; Yu, K.Y.; Spicer, W.E. Photoemission of gold in the energy range 30-300 eV using synchrotron radiation. *Phys. Rev. B* **1976**, *13*, 492. [CrossRef]
31. CasaXPS: Processing Software for XPS, AES, SIMS and More. Available online: http://www.casaxps.com (accessed on 28 November 2023).